JOURNAL OF APPLIED ELECTROCHEMISTRY 17 (1987) 67–76

Current distribution in a two-dimensional narrow gap cell composed of a gas evolving electrode with an open part

YOSHINORI NISHIKI

Research and Development Center, Permelec Electrode Ltd, 1159 Ishikawa, Fujisawa, Kanagawa Prefecture, 252 Japan

KOICHI AOKI, KOICHI TOKUDA, HIROAKI MATSUDA

Department of Electronic Chemistry, Graduate School at Nagatsuta, Tokyo Institute of Technology, Nagatsuta, Midori-ku, Yokohama, 227 Japan

Received 20 December 1985; revised 13 February 1986

On the basis of the observation of gas bubbles evolved by electrolysis, a two-dimensional vertical model cell composed of electrodes with open parts for releasing gas bubbles to the back side is proposed. The model cell consists of two layers. One layer forms a bubble curtain with a maximum volume fraction of gas bubbles in the vicinity of the working electrode with open parts. The other, being located out of the bubble layer, is a convection layer with a small volume fraction distributed in the vertical direction under forced convection conditions. The cell resistance and the current distribution were computed by the finite element method when resistivity in the back side varied in the vertical direction along the cell. The following three cases for overpotential were considered: no overpotential, overpotential of the linear type and overpotential of the Butler–Volmer type. It was found that the cell resistance was determined not only by the interelectrode gap but also by the percentage of open area and in some cases by the superficial surface area. The cell resistance varied only slightly with the distribution of the bubble layer in the back side.

Nomenclature

b	linear overpotential coefficient given by $b = \eta/i$
C	proportionality constant given by Equation 15
d_1	distance between front side of working electrode and separator
d_2	thickness of separator
F	Faraday constant
I	total current per half pitch
i	current density at working electrode
i_0	exchange current density
L	length of a real electrolysis cell
n	number of electrons transferred in electrode reaction
o_p	percentage of open area given by Equation 1
p	pitch, i.e. twice the length of the unit cell, defined by 2(BC) in Fig. 4
q	thickness of bubble curtain, defined by (AM) in Fig. 4
R	gas constant
r_t	total cell resistance
r	unit-cell resistance defined by $(V - V_{eq})/I$
r_{rs}	residue of r from sum of r_0 and r_η
r_0	ohmic resistance of solution when $o_p = 0$
r_η	resistance due to overpotential when $o_p = 0$
s	electrode surface ratio or superficial surface area given by Equation 2 for the present model
T	absolute temperature
t	thickness of working electrode defined by EF in Fig. 4
V	cell voltage

0021-891X/87 $03.00 + .12

V_{eq} open circuit potential difference between working and counter electrodes
v solution velocity in cell
v_0 solution velocity at bottom of cell
w width of working electrode, defined by 2(DE) in Fig. 4
x abscissa located on cell model
y ordinate located on cell model
α anodic transfer coefficient
β linear overpotential kinetic parameter defined by $b/[\varrho_{bc}(p/2)]$
dy infinitesimally small length on the boundary
ε volume fraction of gas bubbles in cell
ζ dimensionless cell voltage defined by $nF(V - V_{eq})/RT$
η overpotential at working electrode
Λ Butler–Volmer overpotential kinetic parameter defined by $[nFi_0\varrho_{bc}(p/2)]/RT$
ν coordinate perpendicular to boundary of model cell
ϱ_1 resistivity of bubble-free solution
ϱ_2 resistivity of separator
ϱ_{bc} resistivity of bubble curtain
ϕ potential in cell

1. Introduction

Industrial electrolysis in production-type cells is almost always accompanied by gas evolution. Evolving gas bubbles can be removed from the interelectrode gap through voids or holes which are fabricated in electrodes. In order to promote gas removal from the interelectrode gap, several types of electrode geometries with holes have been devised [1–7]. The simplest technique of reducing the cell voltage is to make the interelectrode gap small. The electrode in a well-developed cell is frequently located so that it may come in contact with a separator made of ion-exchange membranes. Even in cell configurations with such high performance a bubble curtain [8–10] is formed around the electrode causing an increase in ohmic drop. The bubble curtain may have a high volume fraction of gas bubbles and a resistivity which is several times larger than that of the bubble-free solution. On the other hand, in the back side region of the electrode, the volume fraction of gas bubbles may be small because forced convection sweeps gas bubbles to the outlet of the cell. Therefore the resistivity in this region is close to or a little more than that of bubble-free solution.

In this report a two-dimensional model cell with gas evolution is proposed, involving the difference between the resistivity in the bubble curtain and that in the forced convention region. The primary and the secondary current distributions and the cell resistance in this model cell are computed by the finite element method.

2. Observation of gas bubbles

In order to set up a model gas-evolving cell it is necessary to observe and comprehend the behaviour of evolving gas bubbles and, hence, we constructed an electrolysis cell on a laboratory scale as illustrated in Fig. 1. The cell construction, the apparatus and the experimental procedure are described below.

An electrolysis cell with four compartments was constructed so that evolution of gas bubbles could be readily viewed. These compartments were separated by three sheets of ion exchange membrane, as illustrated in Fig. 1. The first compartment had a working electrode DSA (5 × 25 cm exposed) with open parts to which a transparent Nafion membrane (du Pont Type 120) was mechanically attached. The surface of the membrane was scraped with emery paper in order to minimize adhesion of the gas bubbles on the membrane. Pyrex glass was placed at the back of the compartment in order to observe gas bubbles evolving in the back side of the electrode. The second and the third compartments had nickel counter electrodes. The fourth compartment was surrounded by the three compartments and Pyrex glass. Since gas bubbles are free in this compartment, only the gas bubbles evolving in the region between the working electrode and the membrane can be observed through the Pyrex glass. The current from the working electrode flows equally into the two counter electrodes. Hence the current distribution at the working electrode may be relatively uniform in the horizontal direction. Constant current was

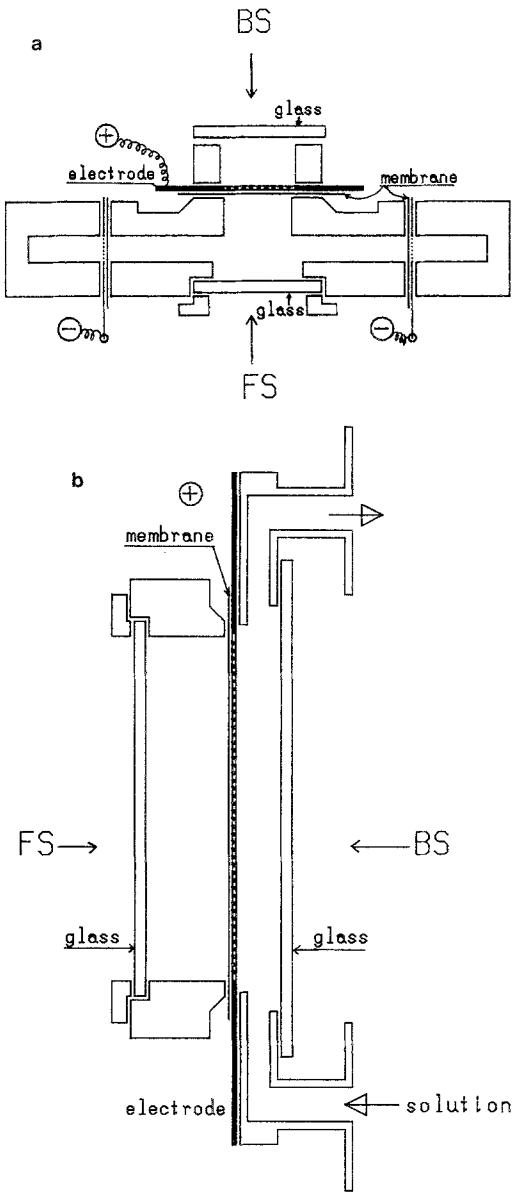

Fig. 1. The top (a) and the side (b) views of the four-compartment cell.

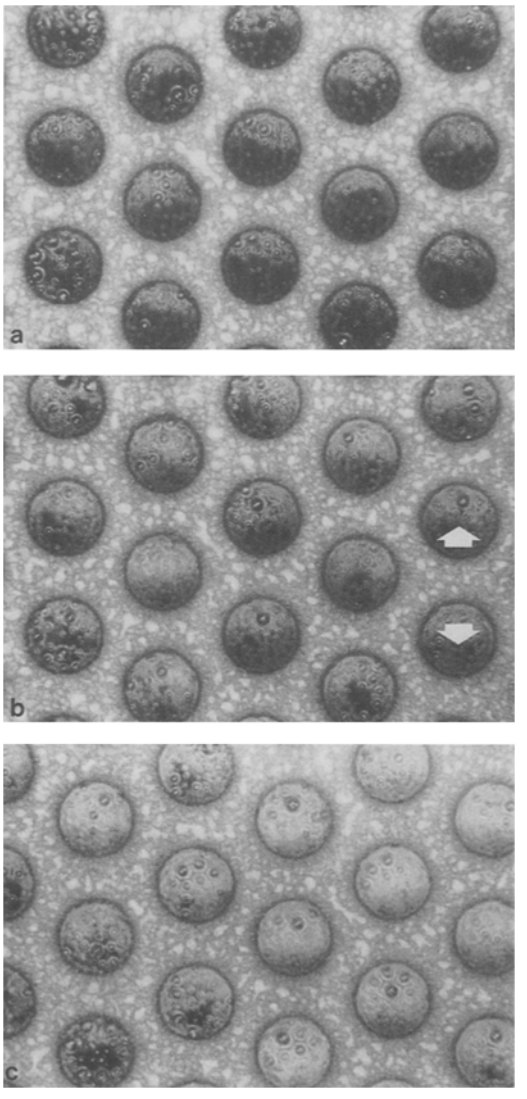

Fig. 2. Photographs of chlorine gas bubbles taken from the front side when the inlet solution velocity was 5 cm s^{-1} and current densities were (a) 0.1, (b) 0.2 and (c) 0.3 A cm^{-2}. Distance between arrows = 3 mm.

supplied by two 2030 regulated d.c. power supplies, 0–25 V, 0–30 A (Fuji Electric MFG, Tokyo).

The NaCl solution (3.5 M) was supplied at the bottom of the working compartment with a constant velocity. The solution drained at the top of the cell was degassed, was reprepared by addition of saturated NaCl solution and was fed to the bottom. NaOH (2.5 M) was placed in the other three compartments. The cell was thermostated at 80° C by an E5C solid state temperature controller (Omron Tateishi Electronics, Kyoto).

Photographs of the gas bubbles were taken with a SMZ-10 stereomicroscope system (Nikon, Tokyo). The dynamic behaviour of gas bubbles was observed with a DBM-5C high-speed film camera (Milliken, Tokyo) and a high-speed video system (BVH-2700 and BVP-3000 (Sony, Tokyo)).

In Fig. 2a–c three photographs for chlorine

gas bubbles are exhibited. These were taken from the front side (FS in Fig. 1) of the working electrode at the centre of the cell for three values of current densities. The inside of the 2-mm diameter circles in these figures indicates the open part of the working electrode. Gas evolving at the front side of the electrode forms bubbles (visualized as white spots) ~ 0.1 mm in diameter in the interelectrode gap. The bubbles move toward an open part. The open part is crowded with bubbles which have evolved in the interelectrode gap and at the inner wall of the electrode, and some bubbles coalesce into large bubbles in the open part. Small bubbles and coalescent ones are then forced out of the open part to the back side (BS in Fig. 1). Global convection of the solution in the interelectrode gap, which is caused by forced convection, was not observed although local convection was noted. From these observations it is possible to regard the layer crowded with bubbles both in the interelectrode gap and in the open part as a bubble curtain. Comparison of these three figures shows that the volume fraction of gas bubbles does not vary with current density when the current density is higher than $0.2\,A\,cm^{-2}$. The volume fraction of gas bubbles in the bubble curtain is almost constant in the vertical direction when the current density is higher than $0.3\,A\,cm^{-2}$.

Observation of the gas bubbles through the back side (BS) of the cell shows the distribution of gas bubbles in the cell from the bottom to the top of the electrode. The volume fraction of gas bubbles increases with height up the electrode because both gas bubbles forced out through the open parts and those evolving at the back side all accumulated in the layer at the back side. In this layer, solution containing gas bubbles is caused to flow upward in the cell by the forced convection.

The photographs in Fig. 2 are for the electrode perforated in a circular form. We observed similar bubble behaviour for other electrode geometries, e.g. expanded electrodes and louver-type electrodes. Therefore, this bubble behaviour is characteristic of a narrow-gap cell composed of electrodes with open parts.

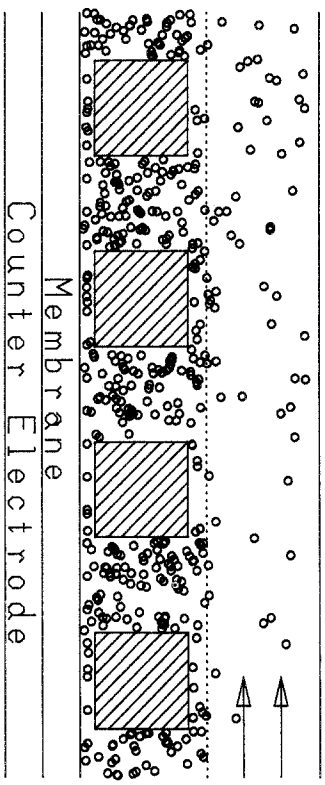

Fig. 3. The two-dimensional two-layer cell model. Hatched squares denote working electrodes with open parts. The region left of the dotted line is the bubble curtain whereas the right region is the convection layer.

3. A choice of model

On the basis of the above observation we present a two-layer model with different gas bubble distributions as shown in Fig. 3. One layer consists of a bubble curtain with a high volume fraction of gas bubbles. The volume fraction of gas bubbles is almost uniformly distributed in this layer and hence the resistivity is also uniform. The layer includes the working electrode with open parts, which is located very closely to the membrane. The model of the working electrode is the same as that introduced previously [11, 12]. Upward convection of the solution in this layer is negligible. The other layer consists of convecting solution with a small volume fraction of gas bubbles, being located outside the bubble curtain. In this layer the volume fraction of gas bubbles increases with height up the cell. It is, however, assumed to be uniformly distributed in the direction normal to

the counter electrode. This layer plays a role in carrying away gas bubbles which are forced out of the bubble curtain.

The model cell is composed of combinations of a unit cell shown in Fig. 4. Since practical cells often have more than a hundred repetitions of the unit cells, the whole cell resistance may be represented by a parallel series of each unit cell resistance which can be regarded as uniform. When the volume fraction of gas bubbles increases with height up in the cell the smooth variation of the resistivity in the whole cell can be treated as a staircase variation, having small increments.

The resistivity in the bubble curtain, ϱ_{bc}, is always higher than that in the convection layer, ϱ_1, and may be in the range $\varrho_1 \leqq \varrho_{bc} \leqq 10\varrho_1$ by estimation from Bruggemann's equation [13]. On the other hand, the resistivity of the membrane, ϱ_2, is often higher than ϱ_{bc} by roughly one order of magnitude. In other words, it follows that $\varrho_1 < \varrho_{bc} < \varrho_2$. The membrane resistance

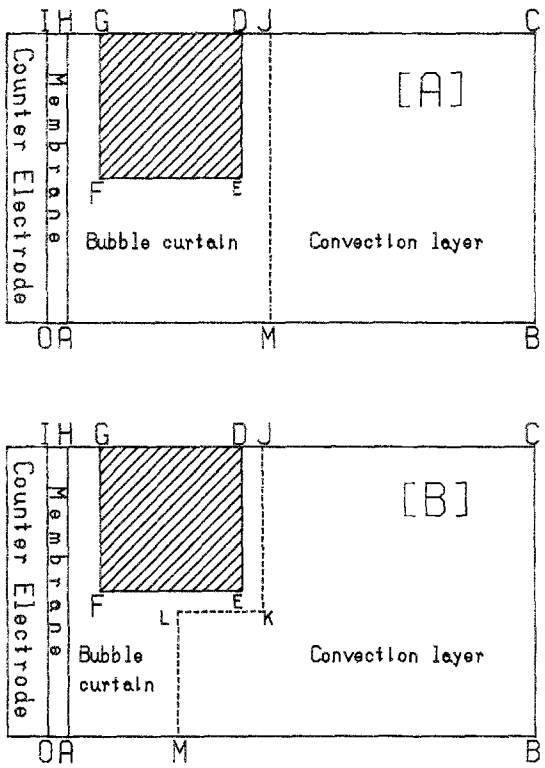

Fig. 4. Two types of unit model cell. The regions AMJDEFGHA in [A] and AMJDEFGHA in [B] are the bubble curtain, whereas the regions MBCJM in [A] and MBCJKLM in [B] are the convection layer.

contributes mainly to the ohmic drop in the whole cell if the cell has a narrow gap. Therefore it is expected that variations of the volume fraction of gas bubbles in the convection layer may have a minor effect on the whole cell resistance.

It is difficult to locate unequivocally the boundary between the bubble curtain and the convection layer. Thus two types of boundary forms as shown in Fig. 4 are taken into account. In the model [A], all the open part is involved in the bubble curtain. This model may be effective for the case of a cell with a small percentage of open area. On the other hand, in the model [B] of Fig. 4, the convection layer extends into the open part. Thus the model cell [B] causes gas bubbles to move more rapidly away from the working electrode.

Parameters relevant to the cell geometry are the percentage of open area, o_p, and the superficial surface area, s, defined respectively by

$$o_p = 100(p - w)/p \quad (1)$$

$$s = 2(w + t)/p \quad (2)$$

4. Computation

For the calculation of the cell resistance and the current distribution, the finite element method was employed; this was the same as that used previously [11, 12] except for the following boundary conditions:

$$\varrho_2(\partial\phi_{bc}/\partial x) = \varrho_{bc}(\partial\phi_2/\partial x) \quad \text{(on AH)} \quad (3)$$

$$\phi_2 = \phi_{bc} \quad \text{(on AH)} \quad (4)$$

$$\varrho_1(\partial\phi_{bc}/\partial v) = \varrho_{bc}(\partial\phi_1/\partial v) \quad \text{(on JKLM)} \quad (5)$$

$$\phi_1 = \phi_{bc} \quad \text{(on JKLM)} \quad (6)$$

Applying the Gauss divergent theorem [14] to the Laplace equations in the bubble curtain domain and the convection layer, and combining the resulting equations by use of Equations 3 and 5 yields

$$\varrho_2 \int_{DEFG} iv\,d\gamma + \int_{IO}(\partial\phi_2/\partial v)v\,d\gamma = u_2 + (\varrho_2/\varrho_{bc})u_{bc} + (\varrho_2/\varrho_1)u_1 \quad (7)$$

with

$$u_k = \iint_{\Gamma_k}[(\partial\phi_k/\partial x)(\partial v/\partial x) + (\partial\phi_k/\partial y)(\partial v/\partial y)]\,dx dy \quad (8)$$

where the subscript k denotes 1, 2 or bc. Equations 7 and 8 were numerically solved by the finite element method which has been described previously [11, 12]. A computer program was checked on the basis of the fact that data computed for $\varrho_{bc} = \varrho_1$ were the same as those obtained previously [11, 12].

5. Results and discussion

5.1. *Potential and current distributions*

In Fig. 5a and b the potential distributions in the model cells [A] and [B] are drawn, respectively, for the case of no overpotential, where the

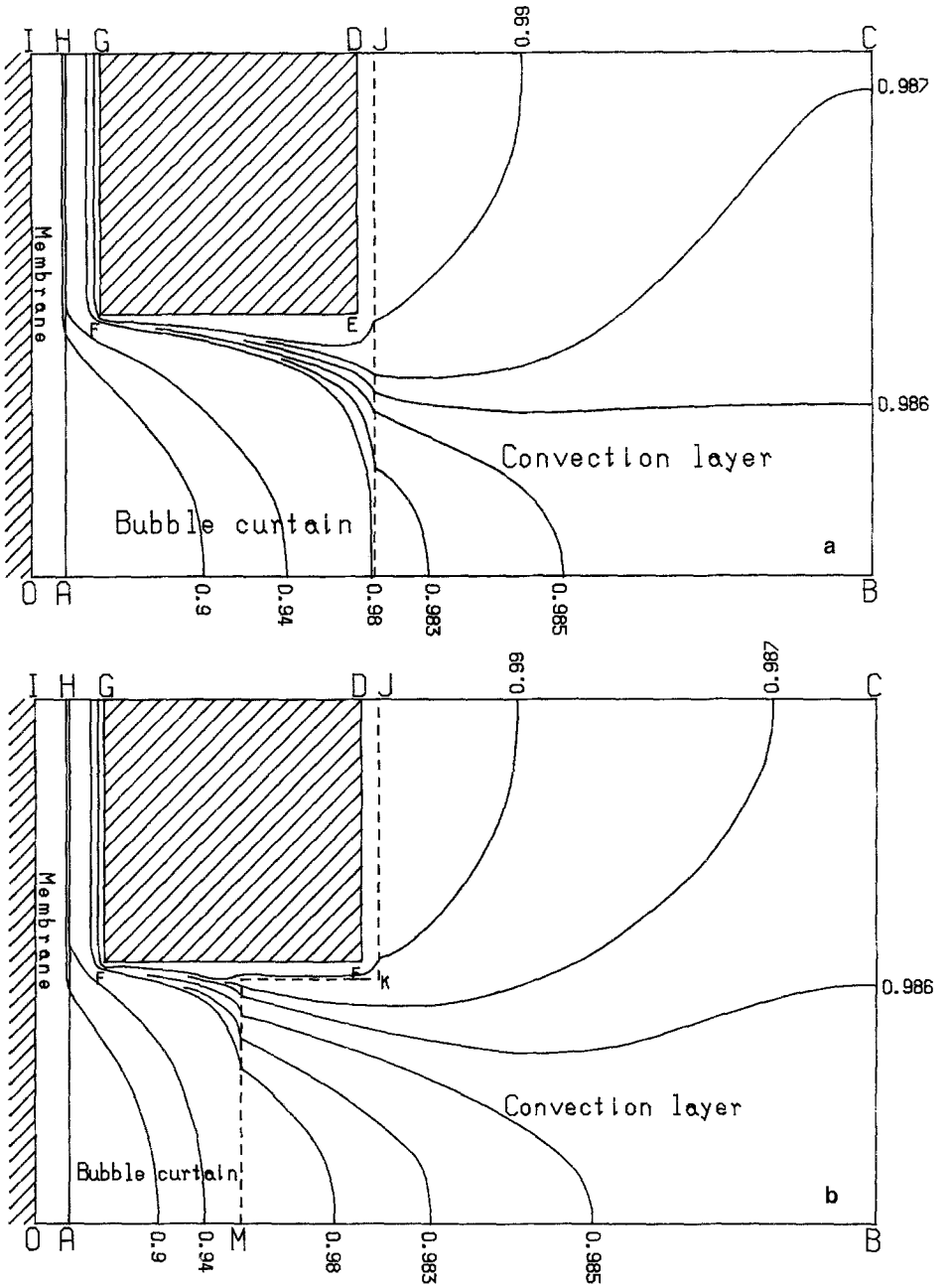

Fig. 5. Potential distributions in the model cells [A] and [B] with the following parameters: $d_1/p = 0.033$, $d_2/p = 0.033$, $w/p = 0.5$, $t/p = 0.25$, (or $o_p = 50\%$, $s = 1.5$), $\varrho_2/\varrho_1 = 200$, $\varrho_{bc}/\varrho_1 = 10$ when the electrode has no overpotential.

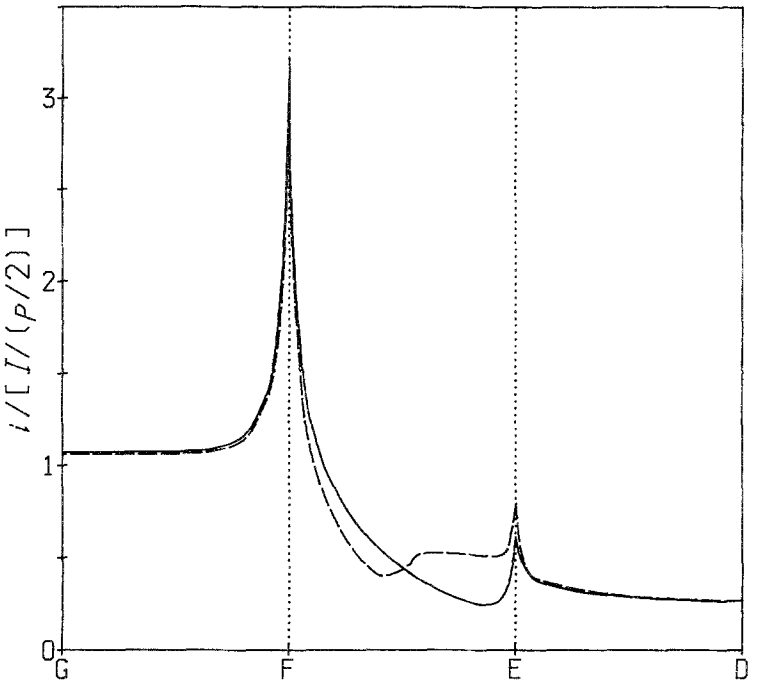

Fig. 6. Current distributions at DE, EF and FG sides for model [A] (——) and model [B] (– – –). The abscissa denotes the distance along the working electrode. Parameters are the same as in Fig. 5.

resistivity of the bubble curtain was taken to be 10 times larger than that of the convection layer. The slope of equipotential lines changes abruptly at the boundary between the bubble curtain and the convection layer due to the sudden change in resistivity. The current distributions for these two model cells are shown in Fig. 6.

In Fig. 7 the partial currents at the back (DE), the middle (EF) and the front (FG) sides are plotted against the dimensionless length, $q/(p/2)$ or (AM)/(BC) in the same model cell as in Fig. 4 when the working electrode has no overpotential. The domain, $q/(p/2) > 0.6$ in Fig. 7 corresponds to the model [A] whereas $q/(p/2) < 0.6$ corresponds to model [B]. When the whole cell is occupied with the bubble curtain, the partition of the current at the front (FG) side is the largest while that at the back (DE) side is the smallest. As the thickness of the bubble curtain decreases, the partition at the back (DE) side increases at the expense of the partitions at the middle (EF) and the front (FG) sides. When values of $q/(p/2)$ becomes less than 0.6 the model changes from [A] to [B], the partition at the back (DE) side becomes almost a maximum and does not vary with $q/(p/2)$. Then the partition at the middle (EF) side increases by the extent of a decrease in the partition at the front (FG) side. All these variations can be explained by the fact that the resistivity in the convection layer is smaller than in the bubble curtain and hence the current flows more favourably in the convection layer than in the bubble curtain.

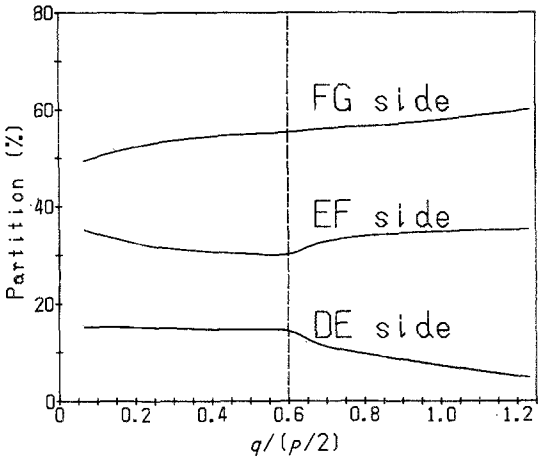

Fig. 7. Variations of the partition of the total current into the currents on the three sides of DE, EF and FG with $q/(p/2)$. The cell geometry is the same as in Fig. 5.

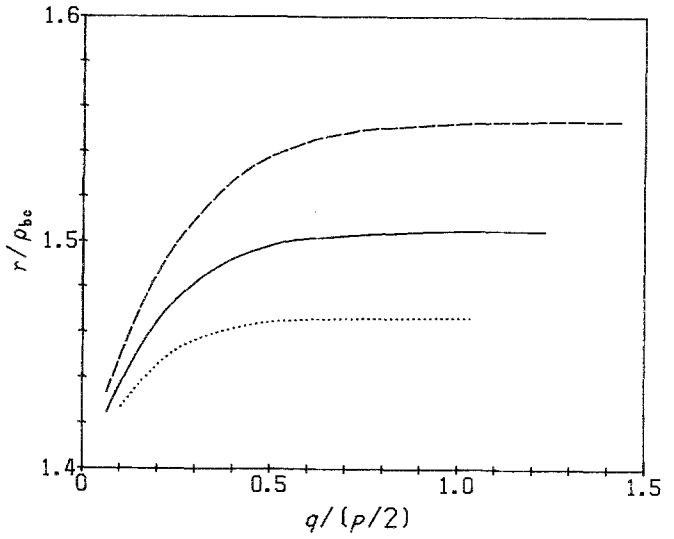

Fig. 8. Variations of the dimensionless cell resistance with $q/(p/2)$ for o_p = 60% (– – –), 50% (——) and 40% (····). The other cell geometry is the same as in Fig. 5.

Where there are no gas bubbles in the cell the partitions of the front (FG), the middle (EF) and the back (DE) sides are 54.2, 37.7 and 8.1%, respectively. Comparison of the curves in Fig. 7 with these values indicates that the role of the back (DE) side in electrolysis cannot be neglected in gas-evolving electrodes.

5.2. *Unit-cell resistance or cell voltage*

In the previous paper [12], the unit-cell resistance, r, was expressed by the following simple sum:

$$r = r_0 + r_\eta + r_{rs} \tag{9}$$

where

$$r_0 = (\varrho_2 d_2 + \varrho_{bc} d_1)/(p/2) \tag{10}$$

It is expected that the cell resistance in the two-layer model cell may also be expressed in a form similar to Equation 9. In the following sections the unit cell resistances for the three cases of no overpotential, linear overpotential and Butler–Volmer overpotential will be obtained.

5.2.1. No overpotential. In Fig. 8 the dimensionless unit-cell resistance is plotted against $q/(p/2)$ for three values of the percentage of open area. For $q/(p/2) > 0.6$ or for the case of the model [A], the cell resistance does not vary with $q/(p/2)$. This finding implies that the convection layer plays a minor role in determining the cell resistance. As the convection layer intrudes into the open part for the model [B], i.e. for $q(p/2) < 0.6$, the cell resistance gradually decreases. Variations of the length of (LM) have little influence on r. Variations of r with $q/(p/2)$ increase with an increase in o_p.

The domain of $q/(p/2)$ in which the cell resistance varies only less than 1% is $q > (d_1 + t/2)$ when $1 \leqq \varrho_{bc}/\varrho_1 \leqq 10$. In these domains of $q/(p/2)$ and ϱ_{bc}/ϱ_1, the cell resistance is independent of the thickness and the resistivity of the bubble curtain. Therefore the cell resistance in the two-layer model can be expressed by the approximate equation for the uni-layer model presented previously [12] in which ϱ_1 is replaced by ϱ_{bc}. Then the cell resistance is expressed by [11]:

$$r = r_0 + 0.333\,(o_p/100)^{2.1}\varrho_{bc} \tag{11}$$

Equation 11 is valid for $o_p < 80\%$, $1 \leqq \varrho_{bc}/\varrho_1 \leqq 5$ and $\varrho_2/\varrho_1 > 20$.

5.2.2. Linear overpotential. Various curves were also observed similar to those in Fig. 8 for the case of linear overpotential for various values of s, o_p, ϱ_{bc}/ϱ_1, ϱ_2/ϱ_1 and the kinetic parameter, β. These showed the variation of r with $p/(q/2)$. Consequently, we found that the convection layer did not contribute to the cell resistance within 2% error if $q > (d_1 + 3t/4)$. The approximate equation for the cell resistance in the previous uni-layer model cell [12] is also valid for

the present two-layer model cell and is given by

$$r = r_0 + \varrho_{bc}\beta/s + (0.59s - 0.62)(1 - 0.51^{\beta})\varrho_{bc} + 0.333(o_p/100)^{2.1} \times 0.51^{\beta}\varrho_{bc} \quad (12)$$

This equation holds for $1.5 \leqq s \leqq 2.5$, $o_p \leqq 60\%$, $q > d_1 + t/2$, $1 \leqq \varrho_{bc}/\varrho_1 \leqq 5$ and $\varrho_2/\varrho_1 > 20$.

5.2.3. Butler–Volmer or Tafel overpotential. Variations of the cell resistance with $q/(p/2)$ were examined for various values of combinations of s, o_p, ϱ_{bc}/ϱ_1, ϱ_2/ϱ_1 and three kinetic parameters, α, Λ and ζ. The contribution of the convection layer to the cell resistance can be neglected when $q > (d_1 + 3t/4)$. Then the approximate equation derived in [12] is valid and is given by

$$r = r_0 + (RT/\alpha nFI)\ln[I/i_0(p/2)] + 0.365\varrho_{bc}(o_p/100)^{2.1} - RT/2nFI \quad (13)$$

where the error involved in this equation is less than 0.6 for $nFIr/RT$ under the conditions $0.3 \leqq \alpha \leqq 0.8$, $\Lambda \leqq 0.4$, $\ln[I/i_0(p/2)] \geqq 2$, $1.5 \leqq s \leqq 2.5$, $30\% \leqq o_p \leqq 60\%$ and $q > (d_1 + 3t/4)$. The condition $\ln[I/i_0(p/2)] \geqq 2$ corresponds to the Tafel region.

In the two-layer model employed here, the resistivity of the bubble curtain and the convection layer changes suddenly at the boundary. However, it is possible to regard the variation of the resistivity as smooth because the resistivity of the convection layer does not contribute to the cell resistance if $q > (d_1 + 3t/4)$.

We have not specifically determined ϱ_{bc} in the above discussion but have assumed that ϱ_{bc} can be expressed by Bruggemann's equation as a function of the volume fraction of gas bubbles and the resistivity of bubble-free solution. The volume fraction of gas bubbles in the bubble curtain may vary not only with the surface characteristics of membranes and of electrodes but also with electrode geometry. Furthermore, the resistivity of bubble-free solution varies with concentration depletion of reactants, which is remarkable in narrow gap cells. Therefore, ϱ_{bc} in Equations 10–13 may involve implicitly the geometrical parameters.

Since the approximate equations for the cell resistance in this model cell are the same as those previously obtained [12], the relative contribution of overpotential and ohmic drop can be described by Equations 39–45 of [12] in which ϱ_1 is replaced by ϱ_{bc}.

5.3. *Characteristics of the whole cell*

5.3.1. The total cell resistance. As described above, the unit-cell resistance is determined by the resistance of the bubble curtain rather than that of the convection layer. Thus the total cell resistance can be given by a parallel combination of the unit-cell resistance on considering variations of ϱ_{bc} with height up in the cell. From our observation of gas bubbles, the volume fraction of gas bubbles in the bubble curtain was almost constant when the current density was higher than 0.3 A cm^{-2}. This finding corresponds to the uniform distribution of ϱ_{bc} over height in the cell. In this case the total cell resistance is expressed by

$$r_t = rp/2L \quad (14)$$

where explicit expressions for r have been given by Equations 11, 12 and 13 depending on the type of overpotential.

5.3.2. The gas bubble distribution. The convection layer has non-uniform gas bubble distribution. In this layer, equations for the mass balance of gas bubbles and of the solution are respectively [15]

$$\mathrm{d}(\varepsilon v)/\mathrm{d}y = Ci \quad (15)$$

$$\mathrm{d}[(1 - \varepsilon)v]/\mathrm{d}y = 0 \quad (16)$$

If the current density in the unit cell does not vary with height in the cell, Equations 15 and 16 can readily be solved, and the solutions for ε and v are given by

$$\varepsilon = yCI/(p/2)/[v_0 + yCI/(p/2)] \quad (17)$$

$$v = v_0 + yCI/(p/2) \quad (18)$$

where y is height in the cell. The gas bubble distribution observed through the back side is expressed by Equation 17. Equation 18 indicates that the velocity increases linearly with height in the cell.

Acknowledgement

The authors wish to express their appreciation for fruitful suggestions by Mr Seiji Nakagawa, President, Permelec Electrode Ltd.

References

[1] Z. Nagy, *J. Appl. Electrochem.* **6** (1976) 171.
[2] J. Jorne and J. F. Louvar, *J. Electrochem. Soc.* **127** (1980) 298.
[3] F. Hine, M. Yasuda, M. Watanabe and M. Kurate, *Soda to Enso* (Soda and Chlorine) **7** (1981) 281.
[4] F. Hine and K. Murakami, *J. Electrochem. Soc.* **128** (1981) 64.
[5] L. J. J. Janssen, J. J. M. Geraets, E. Barendrecht and S. D. J. Van Stralen, *Electrochim. Acta* **27** (1982) 1207.
[6] F. Hine, M. Yasuda, Y. Ogata and K. Hara, *J. Electrochem. Soc.* **131** (1984) 83.
[7] C. Elsner and F. Coeuret, *J. Appl. Electrochem.* **15** (1985) 567.
[8] F. Hine, M. Yasuda, R. Nakamura and T. Noda, *J. Electrochem. Soc.* **122** (1975) 1185.
[9] O. Lanzi and R. F. Savinell, *ibid.* **130** (1983) 799.
[10] H. Vogt, *Electrochim. Acta* **26** (1981) 1311.
[11] Y. Nishiki, K. Aoki, K. Tokuda and H. Matsuda, *J. Appl. Electrochem.* **14** (1984) 653.
[12] Y. Nishiki, K. Aoki, K. Tokuda and H. Matsuda, *ibid.* **16** (1986) 291.
[13] D. A. Bruggeman, *Ann. Physik,* **24** (1935) 636.
[14] F. Chorlton, 'Vector and Tensor Methods', Ellis Horwood, New York (1977) p. 92.
[15] Y. Nishiki, K. Aoki, K. Tokuda and H. Matsuda, *J. Appl. Electrochem.* **16** (1986) 615.